ARMY SCIENCE CONFERENCE PAPER

STAMP Security Classification here

18 JUN 1982

(1)

Enter last name of author(s) here

Start here

AD A117305

DTIC FILE COPY

DIELECTRIC WAVEGUIDE ANTENNA (U)

*JOHN BOROWICK, WILLIAM BAYHA
COMBAT SURVEILLANCE & TARGET ACQUISITION LABORATORY
USA ERADCOM

RICHARD A. STERN, RICHARD W. BABBITT
ELECTRONICS TECHNOLOGY & DEVICES LABORATORY
USA ERADCOM

Introduction

This paper will describe the novel design of a non-metallic dielectric waveguide frequency scan antenna. This antenna is capable of frequency scanning a beam over a spatial angle four times greater than that obtained with a conventional slotted metal waveguide antenna design. This is done with the same percentage change in frequency and there is no metallization required of the radiating aperture. The entire radiating aperture and the transmission line are an integral, homogeneous material; no individual assembly of radiating elements to the transmission line is necessary. The absence of metallization not only means that the fabrication procedure has been considerably simplified, but also that the conductor ohmic losses are eliminated.

The antenna is made by cutting grooves into the surface of a dielectric waveguide. The grooves act as radiating elements. This paper will describe the design and test results of several line source antennas that were investigated at Ka Band, for applications in the millimeter wave frequency range.

Background

Antenna beam scanning can be accomplished by several means. Often the simplest expedient is to mechanically scan the antenna by physically moving the entire antenna structure. For system applications where fast and precise beam steering is required, inertialess beam scan is used. Inertialess beam scan is usually accomplished electronically by altering the phase across the radiating aperture with discrete phase

DISTRIBUTION STATEMENT A
Approved for public release;
Distribution Unlimited

DTIC ELECTE JUL 20 1982 S D

B

STAMP Security Classification here

82 07 19 299

STAMP Security Classification here

Last name of author(s) here → BOROWICK, BAYHA, STERN & BABBITT

Start here for all pages after the first

On first page type title of paper here

Author Affiliation City, State

First line →

shifting components or by altering the frequency whereby an inherent phase is attained between individual radiating elements. All the above techniques are used at microwave frequencies. For millimeter wave frequencies (i.e., 30-300 GHz) mechanical scan is used in virtually all systems. Inertialess scanning at millimeter waves is difficult because of the impracticality in size of the components that would be used for beam steering. It is readily apparent to the millimeter wave antenna engineer that new concepts are needed for beam scanning at millimeter waves. (1)

The Combat Surveillance and Target Acquisition Laboratory has recognized the need for new antenna techniques and has been working under a joint internal Army effort with the Electronics Technology and Devices Laboratory to develop a dielectric waveguide line source antenna. This antenna is unique in that the transmission line and the antenna aperture are an integral, homogeneous structure. The dielectric waveguide transmission line is simply grooved with a saw blade so as to form the radiating elements. This is an inherently simple, low cost fabrication process. The integral design of this transmission line - radiating aperture implies a potential for conformal mounting to a curved surface. When these highly desirable fabrication attributes are noted, along with the significant fact that there is a factor of four increase in the spatial scan sensitivity, this design becomes very interesting.

Dielectric Waveguide

The cross section of the dielectric waveguide was designed using the analysis of Marcatili. (2) The cross section dimensions used were a = 0.052" and b = 0.070", which allows only propagation of the lowest order E_{11}^{y} mode, which is shown in Figure 1. The dielectric waveguide was tapered on both ends so as to permit a transition to standard Ka Band waveguide for test purposes. In particular, each dielectric waveguide had an H plane taper at both ends, which served as the transition between the standard TE_{10} metal waveguide mode to the E_{11}^{y} dielectric waveguide mode. By choosing magnesium titanate, a high dielectric-constant material for which the index of refraction n = 4, nearly all of the power flow is confined to the waveguide. The transverse wavenumbers, k_x and k_y, are obtained in our case from the transcendental equations

$$k_x a = \pi - 2 \tan^{-1}\left[(n^2 - 1)k_o^2/k_x^2 - 1\right]^{-\frac{1}{2}} \qquad (1)$$

and

Insert downgrading/ declassification information on first page of paper only →

STAMP Security Classification here

page 2

DTIC COPY INSPECTED 2

STAMP Security Classification here

Enter last name of author(s) here → BOROWICK, BAYHA, STERN & BABBITT

Start here for all pages after the first →

$$k_y b = \pi - 2 \tan^{-1}\left[n^4(n^2-1)k_o^2/k_y^2 - 1\right]^{\frac{1}{2}}, \qquad (2)$$

On first page type title of paper here → respectively, where k_o is the free-space wavenumber corresponding to the operating frequency. The propagation wavenumber k_z is obtained from

Author affiliation City, State →

$$k_z = \left[n^2 k_o^2 - k_x^2 - k_y^2\right]^{\frac{1}{2}}. \qquad (3)$$

First line →

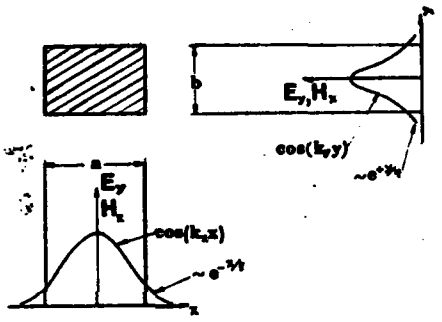

FIGURE 1. E^y_{11} DIELECTRIC WAVEGUIDE MODE

Calculated values of the guide wavelength, $\lambda_g = 2\pi/k_z$, are plotted in Figure 2. A knowledge of λ_g is required in order to proceed to the next step of the design procedure, i.e., a determination of radiating slot spacing, which will, in turn, determine the beam pointing direction.

Dielectric Waveguide Antenna

It is evident from Figure 1 that the E_y and H_x field components are not zero at the edge of the waveguide. Thus there exists a surface wave at the dielectric-air interface. If perturbations are spaced at some periodic interval d along the length of the guide, a radiation field will be created. In our case the perturbations consist of transverse slots cut into the dielectric, of width w and depth t. As indicated in Figure 3, the E-plane beam peak appears at an angle θ with respect to the normal, given by the expression

STAMP Downgrading/ Declassification information on first page of paper only →

STAMP Security Classification here

STAMP Security Classification here

Type first line of author(s) here

Start here for all pages after the first

On first page type title of paper here

Author Affiliation City, State

First line

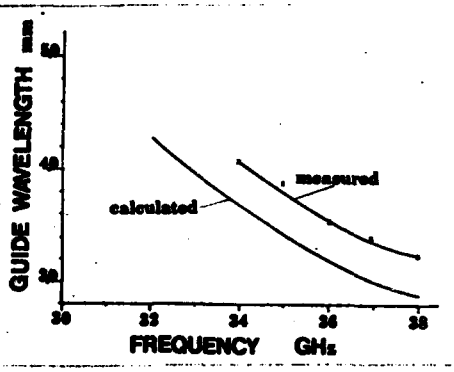

FIGURE 2. GUIDE WAVELENGTH VS. FREQUENCY

$$\sin\theta = \lambda_o/\lambda_g + m\,\lambda_o/d\ , \tag{4}$$

where λ_o is the free-space wavelength corresponding to the operating frequency. It is evident that the beam may be scanned in space by changing the frequency. The quantity m in Eq. (4) is limited to m = -1, -2, -3, . . . corresponding to spatial harmonics in the visible space ($-\pi/2 \leq \theta \leq \pi/2$). For maximum coupling [3], as well as single beam operation from backfire to endfire, the value m = -1 is chosen. The value of d is then limited by the condition

$$\left| \lambda_o/\lambda_g - \lambda_o/d \right| \leq 1. \tag{5}$$

The slots were cut into a slab of dielectric by a precision-controlled diamond dicing saw. The slab was then machined to the finished waveguide dimensions, including the H plane tapers at each end. Table I gives the slot widths and depths studied. Based upon the Marcatili equations for λ_g, and also by considerations which will be given in the next section, the value d = 0.130" was chosen. This slot spacing puts the beam reasonably close to broadside for the frequencies of interest.

As a result of the radiation loss the propagation wavenumber now becomes complex, i.e.,

$$k_z = 2\,\pi/\lambda_g - i\,\alpha\ , \tag{6}$$

STAMP Downgrading/ Declassification information on first page of paper only

STAMP Security Classification here

STAMP Security Classification here

Last last of author(s) here

BOROWICK, BAYHA, STERN & BABBITT

Start here for all pages after the first

On first page type title of paper here

Author Affiliation City, State

First line

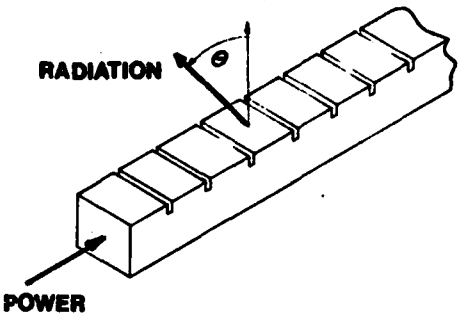

FIGURE 3. DIRECTION OF MAIN BEAM

	w (in)	t (in)
A	0.004	0.006
B	0.004	0.009
C	0.004	0.012
D	0.004	0.015
E	0.004	0.018
F	0.004	0.013
G	0.013	0.013
H	0.020	0.013

TABLE I. SLOT PARAMETERS

where α is the attenuation due to radiation along the length of the array, with $\alpha/k_z \ll 1$. The aperture excitation is therefore exponentially decaying, with the power attenuated equal to the power radiated, P_{RAD}, as given by

$$P_{RAD} = P_o \exp(-2 \alpha L), \quad (7)$$

where P_o is the power incident on the first slot, and L is the array length.

Page numbering/ classification information on first page only

STAMP Security Classification here

STAMP Security Classification here

Author(s) here

BOROWICK, BAYHA, STERN & BABBITT

Start here for all pages after the first

On first page type title of paper here

Author Affiliation City, State

First line

The Experiments

One waveguide was machined to size, as described above, from an unslotted slab. One tapered end was inserted into standard Ka band metal waveguide, using relatively low dielectric constant (ε_r = 2.2) Rexolite as a spacer and support. Due to the large difference in the dielectric constants, the dielectric antenna characteristics were not effected by the Rexolite. The intrinsic insertion loss of the unslotted waveguide was measured, using the set-up shown in Figure 4. The measured loss was found to be 0.5 dB across the 30-38 GHz frequency range.

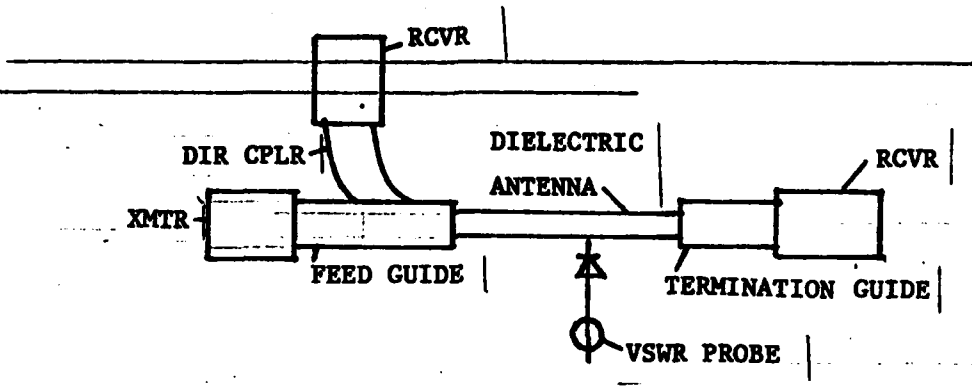

FIGURE 4. TEST SET-UP

Next, a reflecting short was attached to the other taper, and λ_g measured by external probe. These results appear as the upper curve in Figure 2.

Finally, an absorbing load was attached to the other end, so as to absorb any residue fields. Return loss was measured at the input end, and was better than 20 dB across the band, indicating that the combined H plane taper, guide cross section and load were all well matched.

Each slotted antenna was then similarly fitted and tested with the exception of the λ_g probe measurement, due to interference from the near-field radiation caused by the slots. Figure 5 gives some typical results. It is noted that there are loss resonances near 32 GHz and 36 GHz. The higher frequency resonance corresponds to the high reflection loss that occurs when the wavelength in the guide equals the slot spacing. For all antennas tested, it was found that the frequency at the center of the reflection loss curve corresponds to values of λ_g that lie between

Optional downgrading/declassification information on first page only

STAMP Security Classification here

STAMP Security Classification here

BOROWICK, BAYHA, STERN & BABBITT

the upper and lower curves of Figure 2. In general, it was found that the width of the resonance, as measured 3 dB down from the peak of the reflection loss, did not exceed 1 GHz. As the reflection loss at 32 GHz is small (≤ 1%), the lower frequency resonance corresponds to maximum power radiated by the antenna.

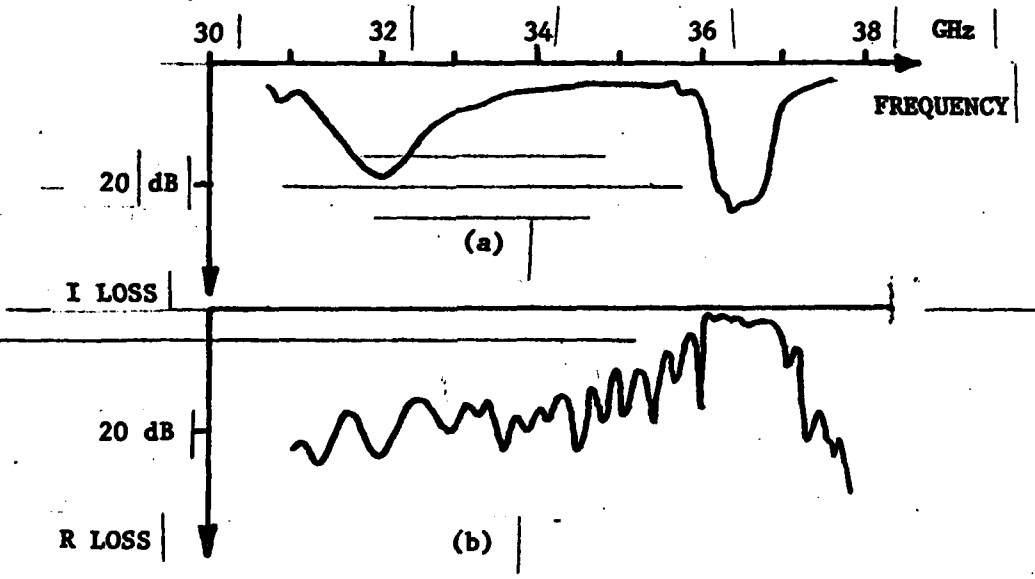

FIGURE 5. TYPICAL LOSS CURVES
(a) INSERTION LOSS
(b) RETURN LOSS

At any given frequency the ratio of net power loss ($P_{NET\ LOSS}$) (i.e., power not delivered to the load) to incident power is, from Figure 5(a)

$$\frac{P_{NET\ LOSS}}{P_o} = 1 - 10^{-I/10}, \qquad (8)$$

where I is measured in dB. Taking into account the intrinsic 0.5 dB broadband loss, the power loss (P_{LOSS}) ratio becomes

$$\frac{P_{LOSS}}{P_o} = 1 - 10^{-I/10} - (1 - 10^{-0.05}) = 0.89 - 10^{-I/10} \qquad (9)$$

STAMP Security Classification here

STAMP Security Classification here

BOROWICK, BAYHA, STERN & BABBITT

Finally, the effect of power reflected back to the generator by the slots must be taken into consideration, so that the radiation loss ratio is

$$\frac{P_{RAD}}{P_o} = 0.89 - 10^{-I/10} - 10^{-R/10}, \qquad (10)$$

where R is the return loss measured in dB from Figure 5(b). Combining Eq. (10) with Eq. (7) we find

$$\alpha = -\frac{1}{2L} \ln (0.89 - 10^{-I/10} - 10^{-R/10}). \qquad (11)$$

Values of α obtained in this way are shown in Figure 6. The curves for antennas C, D, E and F are essentially identical. This appears to be the result of a saturation in the slot-surface wave coupling, as the slot depth is increased.

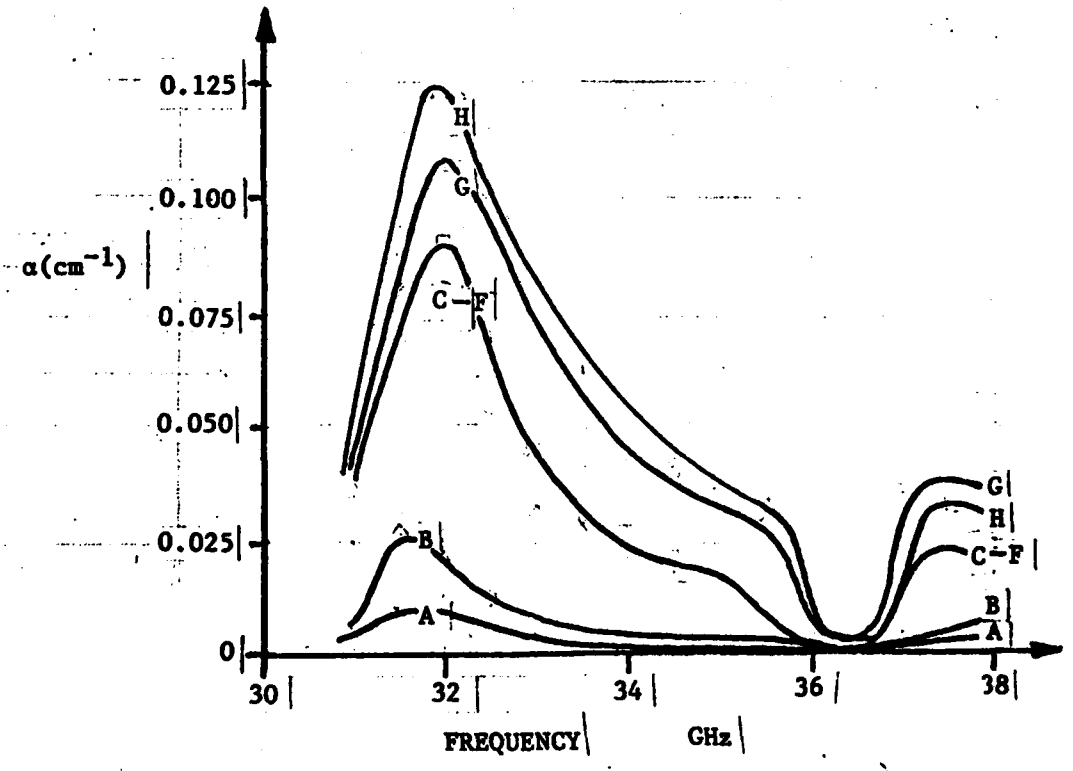

FIGURE 6. SLOT ATTENUATION VS. FREQUENCY

STAMP Security Classification here

STAMP Security Classification here

BOROWICK, BAYHA, STERN & BABBITT

Far field radiation patterns were measured in an anechoic chamber. Several typical E-plane patterns are shown in Figure 7 at 32 GHz, and at 35 and 36 GHz, i.e., either side of broadside. It is noted that the first side lobe levels are typically 12 dB down, close to the theoretical value of 13 dB expected for an exponential illumination. The value of the expected angle of the main beam from the normal is given by Eq. (4), but we have worked this equation backwards, using the observed value of θ, to determine λ_g as a further check. In all cases we again have found λ_g to lie between the upper and lower curves of Figure 2. The 3 dB beamwidth is typically 6° over the 32-37 GHz band, but increases to about 8° near backfire at 31 GHz. The cross-polarization component was measured, and found to be 20 dB down in the main beam.

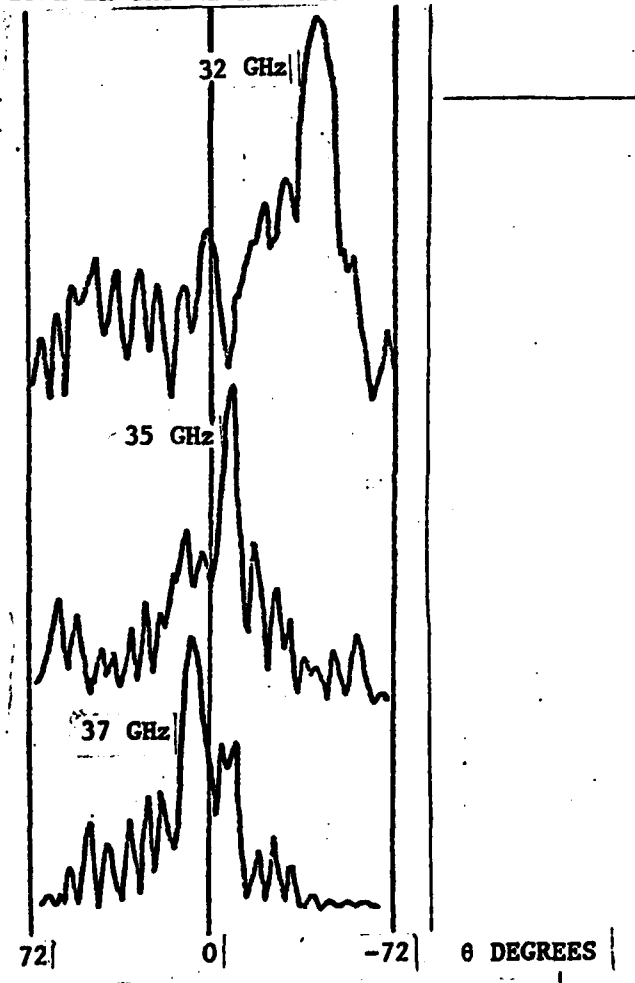

FIGURE 7. TYPICAL PATTERNS

STAMP Security Classification here

STAMP Security Classification here

Insert last name of author(s) here → BOROWICK, BAYHA, STERN & BABBITT

start here for all pages after the first →

The frequency scan characteristic is given by Figure 8; we find for all slot configurations studied a constant scan sensitivity of 11°/GHz, or approximately 4°/(percent change in frequency).

Gain was measured with respect to a standard gain horn. These results are shown in Figure 9.

On first page type title of paper here →

Author Affiliation City, State →

First line →

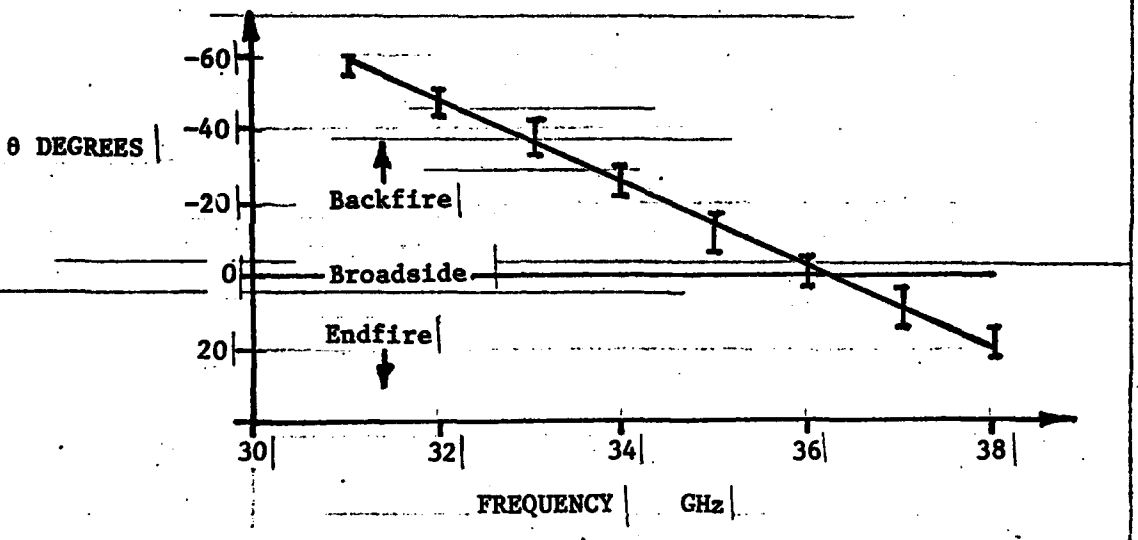

FIGURE 8. SCAN ANGLE VS. FREQUENCY

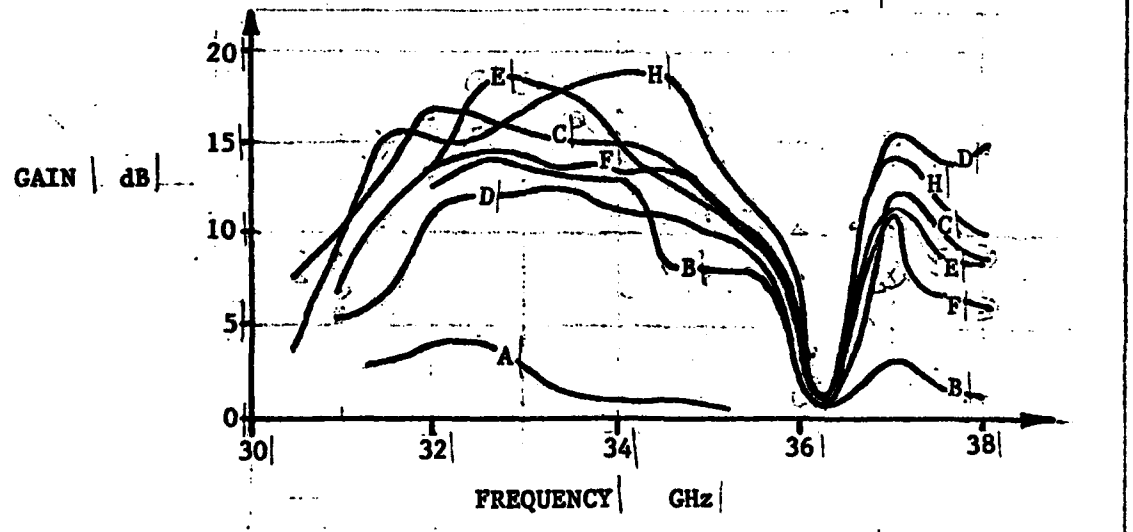

FIGURE 9. GAIN VS. FREQUENCY

STAMP downgrading/ Declassification Information on first page of paper only →

STAMP Security Classificatio here

STAMP Security Classification here

BOROWICK, BAYHA, STERN & BABBITT

Conclusions

Investigations have continued into developing design criteria for a dielectric waveguide line source antenna. The Marcatili analysis has proven to be a reliable guide for the transmission line design. There is, however, no practical design information available permitting the synthesis of a symmetrical amplitude taper along a grooved dielectric waveguide antenna. This investigation presents a measurement procedure that will permit a correlation between the radiating element physical configuration and the radiation properties. Additional data for various slot geometries will continue to be accumulated. A theoretical and emperical relationship will then be made so as to further relate the slot geometry to radiation characteristics. Our investigations have demonstrated that a non-metallic grooved dielectric waveguide can be made to radiate with a well-formed antenna pattern resulting from an exponential amplitude taper. This effort will be extended to permit the design of a lower sidelobe dielectric waveguide slot antenna.

Acknowledgement

The authors wish to thank Mr. William Johnson and Mr. Herbert Daley for their technical assistance, and Mrs. Phyllis Prorok for preparing the manuscript.

References

1. John Borowick, Richard A. Stern and Richard W. Babbitt, "A Small Electronic Scan Angle Antenna for Millimeter Waves", ERADCOM Report DELCS-TR-81-2, September 1981.

2. E.A.J. Marcatili, "Dielectric Rectangular Waveguide and Directional Coupler for Integrated Optics", Bell System Technical Journal, Volume 48, No. 7, pp 2071-2102, September 1969.

3. Johannes Jacobsen, "Analytical, Numerical, and Experimental Investigation of Guided Waves on a Periodically Strip-Loaded Dielectric Slab", IEEE Transactions on Antennas and Propagation, Volume AP-18, No. 3, pp 379-388, May 1970.

STAMP Security Classification here